Available online at www.sciencedirect.com
SCIENCE DIRECT®
Applied Surface Science 229 (2004) 301–310
applied surface science
www.elsevier.com/locate/apsusc

Electron induced reduction on AlF_3 thin films

L.I. Vergara[a,b], R. Vidal[a,*], J. Ferrón[a,b]

[a] *INTEC (Conicet and Universidad Nacional del Litoral), Güemes 3450 CC 91, 3000 Santa Fe, Argentina*
[b] *Facultad de Ingeniería Química (UNL), Santiago 2829, 3000 Santa Fe, Argentina*

Received 6 September 2003; received in revised form 6 September 2003; accepted 3 February 2004

Available online 12 March 2004

Abstract

We studied the modifications introduced in the chemical structure of AlF_3 films by electron irradiation using Auger electron spectroscopy (AES) and factor analysis (FA). We examined the effects of the current density and energy of the electrons on the film composition. We found that the irradiation produces lower aluminum oxidation states (AlF_x with $0 < x < 3$, and Al^0), and that while this effect is independent of the electron density it presents a clear dependence on the primary electrons energy. After comparison of experiments on the dose dependence of AlF_3 and AlF_x reduction, for different energies, with Monte Carlo (MC) simulations, we propose possible mechanisms that lead to electron induced fluorine desorption.

Keywords: Auger electron spectroscopy; Desorption induced by electron stimulation; Factor analysis; Halides; Insulating films

1. Introduction

AlF_3 and AlF_3/LiF alloy thin films are promising materials to be used as inorganic resists for nanometer-scale patterning in electron beam lithography [1–8]. Under electron irradiation these fluorides show radiolysis, i.e. the desorption of the fluoride with the formation of an aluminum metallic layer. The chemical changes that occur during irradiation have been followed by electron energy loss spectroscopy (EELS) [6–8], and the plasmon peaks, that appear in the loss spectra after electron irradiation, indicate the formation of metallic aluminum. However, the basic mechanisms behind the dissociation process are not clearly understood. Possible mechanisms are: the Knotek and Feibelman (KF) [9] Auger stimulated desorption (ASD) of ionically bonded surfaces, the migration of primary electronic excitations to the surface and self-trapping with subsequent ejection of surface atoms [10], and/or the thermal activated diffusion of defects (H and F centres) [2,11–14].

In the present paper, we discuss low energy (0.5–5 keV) electron irradiation experiments on AlF_3 films. The main purpose was to follow, by means of Auger electron spectroscopy (AES), the chemical changes produced by the irradiation. The application of the method of factor analysis (FA) [15] to the Auger spectra helped us to obtain the spectra of the different species formed along the irradiation. This method has been successfully applied to different analysis techniques including AES [16–20], and it is currently included as a standard data treatment procedure in most data treatment packages. The main advantage

* Corresponding author. Present address: University of Virginia, MSE, 116 Engineers Way, Charlottesville, VA 22904-4745, USA. Tel.: +1-434-924-1059; fax: +1-434-924-1353.
E-mail address: rav4n@virginia.edu (R. Vidal).

0169-4332/$ – see front matter
doi:10.1016/j.apsusc.2004.02.008

of FA is its ability to identify linearly independent components appearing in the process under study. Experiments performed with different electron current densities and primary electron energies allow us to draw conclusions about possible mechanisms of AlF_3 dissociation.

2. Experimental setup and data treatment

2.1. Experimental setup

Measurements were performed in a commercial ultra high vacuum (UHV) surface analysis system with a base pressure in the 10^{-10} Torr range. Differentiated Auger spectra of the transitions F–KLL, and Al–$L_{2,3}$VV were acquired using a single-pass cylindrical mirror analyzer (CMA) with a resolution of 0.6% and 2 V_{p-p} modulation amplitude. Fluoride films were deposited 'in situ' from a Knudsen cell charged with anhydrous AlF_3 (CERAC Inc., Milwaukee, Wisconsin, USA, 99.5%). The cell was carefully degassed, and it was shuttered to avoid sample contamination. The films were prepared on top of a p-type GaAs (110) single crystal which was cleaned by cycles of Ar^+ ion bombardment (1 keV) followed by annealing at 500 °C until contamination was below the AES detection limit. The GaAs substrate was at room temperature during AlF_3 evaporations. UHV conditions were kept throughout the evaporations with chamber pressures in the 10^{-10} Torr range. Under these conditions the AlF_3 films present the correct stoichiometry having no preferential surface orientation [21]. The evaporation rate was determined through the attenuation of the substrate signal with deposition time, being a typical value 1.5 Å/min. The analyzed films were 40–50 Å thick. This thickness was large enough to attenuate any Auger signal coming from the substrate, but small enough to prevent sample charging.

The incidence angle of the electron beam was 30° with respect to the surface normal. The beam currents used in the study of electron density dependence in the desorption process were in the range of 5–120 nA, as measured on the sample under a positive bias of 81 V applied to it. The electron beam energy was 2 keV, and the irradiated areas were 7.2×10^{-4} cm^2 for 5 nA and 1.5×10^{-4} cm^2 for 5–120 nA. Auger spectra were acquired during the irradiation without changing the electron beam conditions. Spectra acquisition times were kept as low as possible to minimize changes during the acquisition of an individual spectrum while assuring good signal-to-noise ratios. When studying the energy dependence, the beam current was 5 nA for 2, 3, and 5 keV; and 10 nA for 0.5 and 1 keV. For each energy, the analysis area was determined obtaining the profile of the beam by means of a 0.25 mm diameter Faraday cup. The dose in the irradiated area is likely to be non-uniform since scan paths for the electron beam overlap continuously during rastering. Therefore, the doses determined in these experiments were averaged over the irradiated areas. The dose, ϕ, was calculated as $\phi = J_a \times t_i$, where J_a is the average current density in A/cm^2, and t_i is the total irradiation time in seconds. The average current density was calculated by dividing the electron current by the total rastering area.

2.2. Data treatment

The factor analysis method has been extensively discussed in our previous works [18,19,22–25], therefore, we will limit ourselves to a brief description.

The application of FA to the Auger spectra helped us to obtain the spectra of the different species formed along the irradiation. The first step is the determination of the number of linearly independent factors, i.e. the minimum number of pure components required to describe the complete series of spectra corresponding to the evolution under study. In doing that, we compare the experimental error with the error performed in reproducing the experimental data with a minimum set of factors. This procedure is performed as Auger spectra are added in a sequential way [18], and each time this error surpasses the experimental one a new factor appears in the process. Once the number of independent factors is known, the Auger line shape of each pure component (or base) is determined through a least square fit procedure called target transformation (TT) [15,18]. The final step in FA is the correlation among the obtained bases and actual compounds. Usually, when the base compounds are known this procedure reduces to a simple fingerprint analysis. In the present case the procedure is a bit more complicated, and the way we did it will be explained in detail in the following sections.

3. Results

In Fig. 1, we depict the evolution of the Auger line shape versus electron bombarding dose, that characterize the reduction process of the aluminum fluoride, taking place under the electron irradiation. In the first spectrum we can identify the Auger peaks corresponding to the aluminum $L_{2,3}VV$ (43 eV) and fluorine–KLL (∼650 eV) Auger transitions. The large chemical shift observed for the aluminum transition within the fluoride matrix, as compared to metallic aluminum (Al^0, 65 eV) points out the high oxidation state of the aluminum (Al^{3+}) in this compound. As the irradiation dose increases, the Auger spectra show a surface depletion of fluorine, and strong changes in the Al–LVV line shape. The final state is characterized by a complete disappearance of the fluorine, and a full metallization of the film. Starting from a stoichiometric aluminum fluoride we end up with a pure metallic aluminum film, within the Auger sensitivity and escape depth. The changes observed in the Al–LVV Auger line shape, along the aluminum fluoride reduction, suggest the appearance of different Al oxidation states. The characterization of these states is just one of the main goals of this work.

The spectra depicted in Fig. 1 were taken with a 2 keV, 15 nA, and 20 μA/cm^2 electron beam current and density, respectively. In order to have an idea of the strong sensitivity of aluminum fluoride to electron bombardment we can compare these values with typical electron beam currents (densities) used in AES, which range between 500 and 1000 nA (4000–8000 μA/cm^2).

3.1. Irradiation current density dependence

As a first step to characterize the reduction process we determined its sensitivity to the bombarding electron density. This is shown in Fig. 2 were we display the evolution of the Auger yields (peak-to-peak heights in the differentiated spectra) of fluorine and

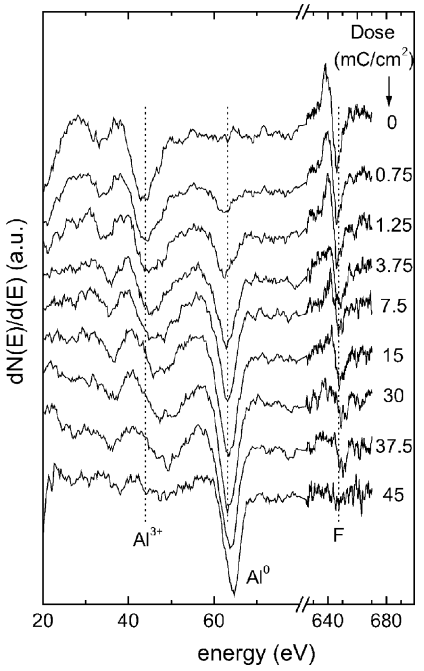

Fig. 1. Auger line shape evolution of fluorine and aluminum peaks during the electron induced desorption process of an AlF_3 film. The electron beam energy and current density used were 2 keV and 20 μA/cm^2, respectively.

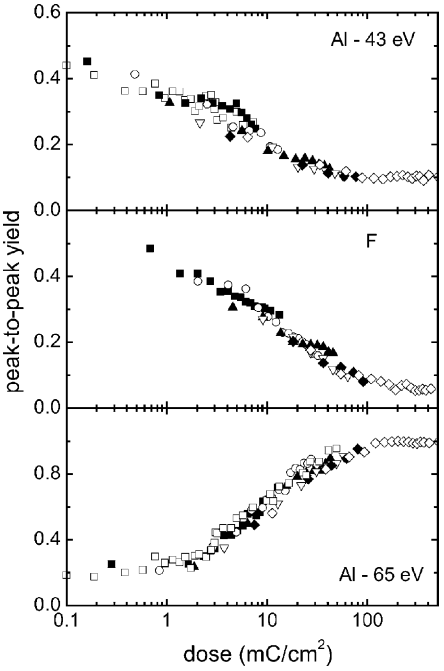

Fig. 2. Auger peak-to-peak yield (normalized to the final Al^0 peak) evolutions for different current densities. The first panel corresponds to the Al peak (43 eV). The second panel corresponds to the fluorine peak (650 eV). The third panel corresponds to the Al peak (65 eV). Current densities: (□) 7 μA/cm^2, (■) 20 μA/cm^2, (○) 60 μA/cm^2, (▲) 140 μA/cm^2, (▽) 280 μA/cm^2, (◆) 560 μA/cm^2, and (◇) 800 μA/cm^2.

aluminum as a function of the electron dose for different electron beam densities. In order to facilitate comparisons among different experiments, all peaks were normalized to the final Al^0 one. For Al we show the evolution of both Auger peaks, i.e. those appearing at 43 and 65 eV.

As we already stated, the electron induced reduction process is characterized by the fluorine depletion and the aluminum reduction, i.e. the disappearance of the 650 eV (F–KLL) and the 43 eV (Al–LVV) Auger peaks and the appearance of the Al 65 eV one. From the results summarized in Fig. 2, we can conclude that the chemical changes induced in the aluminum fluoride, as a consequence of the energetic electron bombardment, are independent of the electron beam density. It is clear that the analysis based on the peak-to-peak evolution is only qualitative, since at this stage we cannot resolve the different compounds present along the reduction process. However, based on a more detailed analysis by FA we arrived to the same conclusions. Therefore, in the rest of our work we used a fixed electron beam density (7 μA/cm^2), which was chosen to get a smooth evolution of the Al reduction process, compatible with the application of the FA method.

3.2. Factor analysis results

In Fig. 3, we summarize the application of the FA method to the evolution of the Al–$L_{2,3}$VV Auger transitions, along the electron beam irradiation process. In Fig. 3(a) the sequential analysis of the error evolution is depicted. In this case, the sequential analysis is performed in reverse order, i.e. starting from the final situation, where we can ensure the existence of only one factor, Al^0. As described in Section 2.2, we start the reconstruction of the data matrix with only one factor (Auger independent spectrum). The need to add a second factor appears when the error in the reconstruction of the data matrix overcomes the experimental error. The physical meaning of this new factor is just the appearance of a different Al oxidation state in the reduction process. The sequential analysis gives in this case three independent factors for the whole Al reduction process. As we know one of these factors (the final one, Al^0), we can apply the TT to determine the other unknown components (Section 2.2). The results are shown in Fig. 3(b) and (c), where we depicted the basis and the evolution of the corresponding weights along the reduction process. Two of the basis are easily identified as Al^0 and Al^{3+}, while the remaining one shows features of an intermediate oxidation state (AlF_x with $0 < x < 3$). This compound is characterized by two different Auger peaks, which are shifted from the Al^{3+} and Al^0 ones. We should here emphasize that the Auger line shape of the new compound is by no means a linear composition of the two already known Al–$L_{2,3}$VV transitions (Al^0 and Al^{3+}). In fact, the first and most powerful capability of factor analysis is just

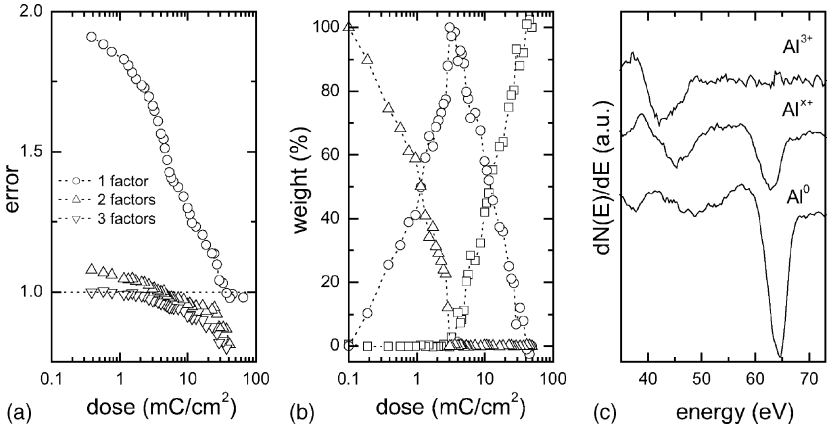

Fig. 3. (a) Evolution of the error (normalized to experimental error) vs. irradiation dose considering only one factor (○), adding a second factor (△), and including a third factor (▽). (b) Evolution of the weights of each component along the desorption process: AlF_3 (△), AlF_x (○), and Al^0 (□). (c) Bases obtained through FA.

the detection of the linearly independent components. Finally, the weight evolution of the three different compounds (Fig. 3(b)), shows the step by step reduction of AlF_3. The process starts with the transformation of Al^{3+} in Al^{x+}, and only when this transformation is completed the following reduction step, conversion of Al^{x+} into Al^0, begins.

3.3. Electron energy dependence

In Fig. 4, we present the weight of the different compounds versus irradiation dose curves, obtained through FA of the Auger line shape evolution during electron beam irradiation, for five different primary energies, namely 0.5, 1, 2, 3, and 5 keV. The evolution of each compound AlF_3, AlF_x and metallic Al is shown separately. In all the profiles we observe, as in the evolution shown in Fig. 3(b), the fall down of the AlF_3 phase from the beginning of the irradiation, the growth of the AlF_x phase followed by its fall down, and the appearance of metallic Al. A clear energy effect can be observed in this process, the lower the electron bombardment energy, the lower the dose required for the appearance of metallic Al, and for the disintegration of the AlF_3.

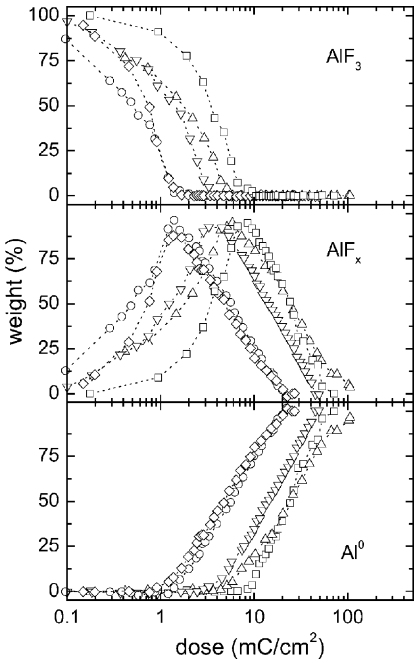

Fig. 4. Evolution of the weights of each component along the desorption process for different electron energies: (□) 5 keV, (△) 3 keV, (▽) 2 keV, (○) 1 keV, and (◇) 0.5 keV. Upper panel: AlF_3, medium panel: AlF_x, lower panel: Al^0.

4. Discussion

4.1. Chemical products of the electron irradiation

The results presented above show the extreme sensitivity of AlF_3 to electron irradiation. In fact, for doses much lower than the usual ones in electron spectroscopy analysis, the irradiation produces a rapid fluorine depletion and strong changes in the chemical state of Al, as revealed by the changes in the Al-LVV Auger transition line shape. The chemical processes induced by the irradiation appear to be independent of the electron beam density but they are clearly dependent on the primary electron energy. The application of the FA method gives us a full picture of the reduction process. The process is characterized by the presence of three independent components (see Fig. 3). Two of these components are identified as Al^{3+} (43 eV) or aluminum in the trifluoride and metallic Al (65 eV), in Fig. 3(c). The remaining component (AlF_x) is characterized by two main peaks in the Auger spectrum. It is known that aluminum forms three fluorides, AlF_3, AlF_2, and AlF. AlF is not known in the condensed state, since at normal temperatures it quickly disproportionates into AlF_3 and Al [26,27]. AlF_2 has been detected in the high temperature equilibrium between aluminum and its fluorides [28]. On the other hand, a simple Auger energy fingerprint analysis of the $L_{2,3}VV$ transition for AlF and AlF_2 using their molecular orbitals calculated through a commercial code (GAUSSIAN) [29], shows that while the $L_{2,3}VV$ transition for AlF has three peaks, for AlF_2 has only two peaks, as expected. While the lack of Auger reference spectra for aluminum fluorides in oxidation states lower than 3 prevents us from a complete identification of the remaining component (AlF_x) the facts mentioned above hint that $x = 2$.

4.2. Energy dependence of the chemical induced process

The results depicted in Fig. 4 shows, as it was already mentioned, a clear energy dependence of

the AlF_3 reduction process induced by the electron bombardment. The efficiency of the electron irradiation to reduce the AlF_3 increases as the impinging energy goes down along the whole energy range analyzed in this work (0.5–5.0 keV). This effect may be noticed, for instance, by observing the lower threshold doses needed for the appearance of the metallic Al Auger transition at lower energies, as well as through the faster transformation of AlF_3 into AlF_x under the same conditions. The type of relationship amongst the concentration of the different compounds appearing during the irradiation, the dose, and the energy of the primary electrons is seen clearly when the data shown in Fig. 4 are represented in a semilog plot. This is shown in Fig. 5 where we represent the decay of the AlF_3 and AlF_x components into AlF_x and Al^0, respectively. We only show the decays for two primary energies (0.5 and 5 keV) to have a clearer view. The decay of AlF_x into Al^0 follows an exponential law, and the slope of this line gives the cross-section related to this process, hereinafter σ_3. On the other hand, the reduction of AlF_3 into AlF_x proceeds in

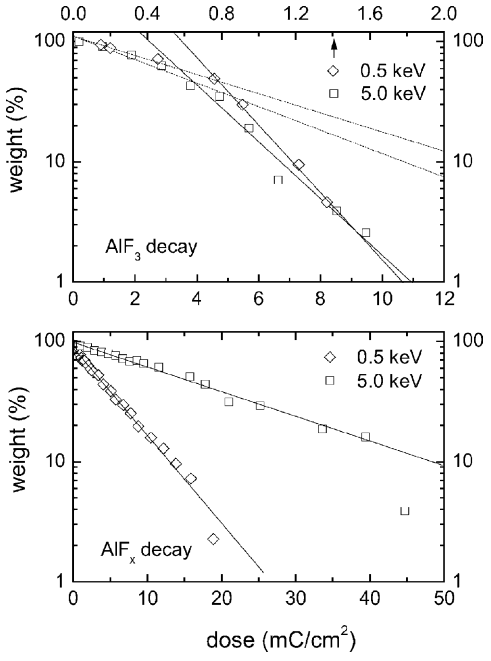

Fig. 5. Evolution of the weights for 0.5 and 5 keV. Upper panel: decay of AlF_3 into AlF_x, the top dose scale applies to 0.5 keV while the bottom one applies to 5 keV. Lower panel: decay of AlF_x into Al^0.

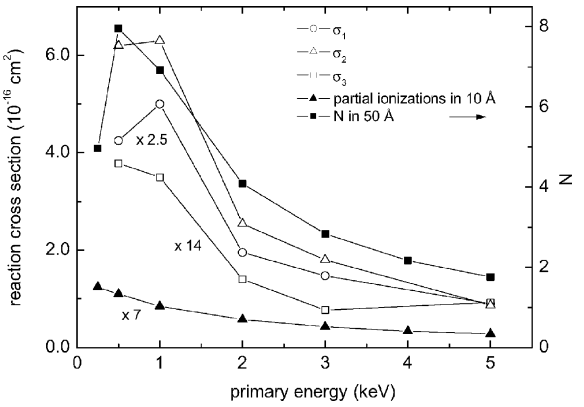

Fig. 6. Primary electron energy dependence of the different reaction cross-sections (left scale): (○) $\sigma_1 \times 2.5$, (Δ) σ_2, and (□) $\sigma_3 \times 14$. Monte Carlo simulation results (right scale) for the number of ionizations produced by a primary electron: (▲) partial ionizations × 7 (see text) in 10 Å and (■) total ionizations in 50 Å. σ_1, σ_3 and the partial ionizations have been multiplied by an arbitrary factor to have a better view.

two steps. First, there is a slow process characterized by a cross-section, namely σ_1, until a critical dose is reach, ϕ_c, then, the reduction process accelerates until all the AlF_3 is transformed into AlF_x. This step is represented by a larger cross-section, $\sigma_2 > \sigma_1$.

In Fig. 6, we depict the primary electron energy dependence of the three before mentioned reaction cross-sections. They have almost the same energy dependence but their relative magnitude is quite different. Thus, σ_2 is about 3.3 times σ_1, and this one about 7.1 times σ_3. In practical terms this means that after the reduction of AlF_3 into AlF_x it takes much more time to reduce the fluoride further into metallic aluminum.

The electron stimulated desorption (ESD) on ionically bonded surfaces is usually explained on the basis of the Knotek and Feibelman [9] model for the Auger stimulated desorption. The ASD in a maximal valency ionic compound is produced, according to the KF model, by the repulsive Madelung potential that appears after an Auger transition that changes the sign of the anion charge. In an ionic compound, like AlF_3, electrons are spatially accumulated around F anions, while the Al is nominally ionized down to the noble gas configuration [9] Al^{3+} (maximal valency). If an energetic electron ionizes an aluminum (fluorine) inner shell, the dominant decay will be an inter-atomic (intra-atomic) Auger process involving two F electrons

and leaving both F and Al positively charged giving place to the F expulsion. We have then that within the KF model, the energy dependence of the electron induced F depletion (or Al reduction) should be related to the energy dependence of the inner shell ionizations produced per incident electron. However, we found in our experiments some evidence that lead us to conclude that other mechanisms of electron stimulated desorption from AlF_3 may be active.

In order to understand the energy dependence of the different reaction cross-sections and gain insight about the possible mechanisms involved in the ESD of fluorine, we study the way the primary electron energy is deposited in the fluoride film. To do that we performed a simplified Monte Carlo (MC) calculation to simulate the energy deposition process in an AlF_3 film. The MC code used along this work was previously applied to model electronic energy deposition in solid argon thin films by keV electrons [30], and details of the simulation can be found there. In our model the electrons can interact with the atoms elastically or inelastically. Differential and total elastic cross-sections were calculated using the partial wave expansion method [31], and inelastic scattering was calculated using the Gryzinski excitation function, using the Al L_1, Al $L_{2,3}$, F L_1 levels, and an effective valence level. The binding energy of this last level was fixed in order to fit the total inelastic cross-section calculated using Tanuma et al. [32] for AlF_3. The MC simulation gave us the depth distribution of ionizations for each electronic level and also the deposited energy depth profile per primary electron. In our calculation we considered a 50 Å thick AlF_3 film supported onto a Ge substrate to take into account, in a simplified way, the substrate effects.

The results of the MC simulation are summarized in Fig. 6 and Table 1, shown together with the energy dependence of the reaction cross-sections. The inner shell ionizations produced by the impinging electrons in the analyzed zone (Auger escape depth, ~10 Å) and the number of total ionizations, i.e. including valence ones, along the whole film are depicted in Fig. 6. A close relationship between the energy dependence of the reaction cross-sections, and the total number of ionizations in the 50 Å thick AlF_3 film, is observed in this figure. This correlation is shown clearly in Fig. 7, where we plot the three reaction cross-sections as a function of the total number of holes (ionizations, N) produced by one electron. The slopes of these straight lines are shown in Table 1.

The crucial point we should emphasize here is the fact that the reaction cross-sections are not proportional to the number of inner shell ionizations produced within the Auger escape depth (see Fig. 6), as it should be within the KF model, but to the total number of holes produced along the whole film. These results show that KF mechanism does not work, at least alone, for the AlF_3 case, and since holes produced far beyond the Auger escape depth affect the ESD, a diffusion mechanism for such holes needs to be considered. Within a diffusion model, our results could be explained considering that the surface is a perfect trap for the reaction centers that lead to fluorine desorption, and the fluoride–GaAs interface is a perfect reflector

Table 1
Results of the dose and energy dependence fitting of the FA results of Fig. 4 to a simple exponential model of AlF_3 and AlF_x degradation under electron irradiation

E (keV)	AlF_3 decay			AlF_x	Monte Carlo results (total ionization/electron)
	σ_1 ($\times 10^{-16}$ cm^2)	ϕ_c (mC/cm^2)	σ_2 ($\times 10^{-16}$ cm^2)	σ_3 ($\times 10^{-17}$ cm^2)	
0.25	–	–	–	–	4.97
0.5	1.7 ± 0.1	0.77	6.2 ± 0.2	2.7 ± 0.06	7.95
1.0	2.0 ± 0.1	0.86	6.3 ± 0.1	2.5 ± 0.06	6.92
2.0	0.78 ± 0.03	1.65	2.54 ± 0.06	1.0 ± 0.02	4.09
3.0	0.59 ± 0.03	3.36	1.8 ± 0.1	0.55 ± 0.1	2.84
4.0	–	–	–	–	2.17
5.0	0.36 ± 0.06	3.8	0.9 ± 0.1	0.7 ± 0.2	1.76
	0.24 ± 0.02		0.79 ± 0.05	0.33 ± 0.03	

The sixth column shows results of total ionizations/electron (N) for an initially 50 Å thick AlF_3 film calculated using Monte Carlo simulation. The last row shows the slopes of the straight lines $\sigma = bN$.

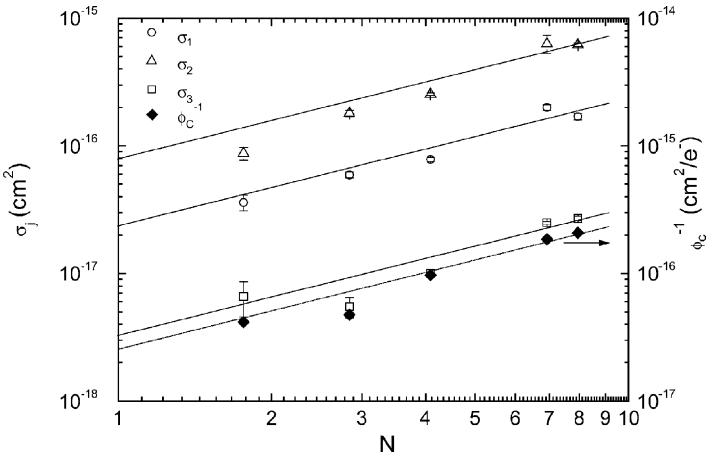

Fig. 7. Correlation between reaction cross-sections and total number of ionizations (N) as obtained from a Monte Carlo simulation of electrons interacting with a 50 Å thick AlF_3 film. Cross-sections that describe the transformation of AlF_3 into AlF_x: (○) σ_1 and (△) σ_2. Idem for the transformation of AlF_x into Al^0 (□) σ_3. Reciprocal of the critical dose (ϕ_c) at which reaction 2 takes place (◆).

for these centers, i.e. every hole along the film contributes to the fluorine ESD.

This is not, of course, the first case where other mechanisms, different than the KF, should be included to explain ESD experiments. For instance, Golek and Sobolewski [14] measured thresholds of ESD for LiF thin films and confirmed that ASD contributes to the desorption process, but also found lower energy thresholds consistent with a ''defect-mediated desorption model'' [13]. There are basically two mechanisms that have been proposed to explain halogen desorption involving the diffusion of holes and excitons, and/or reactions centers [10–13]. They are the thermal desorption process, attributed to the diffusion of defects (H and F centers) created in the bulk of the material by the self-trapping of valence holes [11], and the hyperthermal halide emission explained by the diffusion of holes and excitons to the surface that after self-trapping leads to halide emission. The diffusion lengths of these mechanisms ranges, at room temperature, from 75 Å for H centres to 140 Å for holes and exciton diffusion [11] in KBr films, in total agreement with the dimension of our thin films.

There is another interesting parameter that can be calculated relating the ionization process with the process that leads to a certain reaction. This number is the probability of the reaction j, p_j, after a hole has been created. The density of reaction centers would be: $n_j = p_j n$ where n is the hole density. When the dose is not very large the relation between p_j and the respective reaction cross-section, σ_j, can easily been calculated as: $p_j = \sigma_j n_0/N$, where n_0 is the volume density of AlF_3 molecules (2.2×10^{22} mol/cm^3) times the thickness of the film. Since the relationship between σ_j and N is a constant that does not depend on the primary energy we can calculate the reaction probabilities as 26, 87, and 3.6% for reactions 1, 2, and 3, respectively.

We have then that the fluorine ESD is characterized by three different reaction processes. Two of them lead to the transformation of AlF_3 to AlF_x and the remaining one is the transformation of AlF_x into metallic Al. All these processes have the same primary electron energy dependence, but quite different absolute values. We previously shown (see Table 1) that the critical dose, i.e. the dose after which the transformation of AlF_3 into AlF_x precipitates, is energy dependent. But, what about the total number of ionizations, that correlates the dose and the ionization efficiency, occurring at these critical dose? In Fig. 7, we shows that N is proportional to the reciprocal of the critical dose (ϕ_c) being $N\phi_c$ a constant equal to $(3.9 \pm 0.2) \times 10^{16}$ ionizations/cm^2. This fact just means that the number of holes needed for going from the process characterized by σ_1 to that characterized by σ_2 is a material constant. The same (not shown) occurs for the other critical dose, i.e., changing from σ_2 to σ_3. But, while in the last case we can easily understand that a

fixed number of holes is needed to completely transform AlF_3 into AlF_x, the change from the σ_1 regulated process to the σ_2 one is a bit more puzzling. Starting from the fact that the change is only related to the reaction rate, being the reaction always the same, the system acts as if the presence of a certain number of holes, or AlF_x centers, catalyzes the following reaction. Here again, we can certainly accept such kind of argument thinking in diffusion limited processes more than in a KF based process. Finally, the lower value of σ_3 may be understood on the basis of a larger stability of the AlF_x molecules under electron irradiation. As the Al atom in AlF_x is partially charged, the sensitivity of the molecule to experiment an ESD event may be lower.

5. Conclusions

We have characterized the electron induced reduction process of aluminum fluoride. We found that three different Al oxidized states appear along the whole process. We identified these states, through factor analysis and an energy fingerprint, as Al^{3+}, Al^{x+}, and Al^0, where x is likely ~ 2. We determined that the desorption (reduction) process depends on the primary electron energy and dose, but it is independent of the electron beam density.

The decomposition of AlF_3 into AlF_x as a function of the dose takes place in two steps that can be described with two reaction cross-section (σ_1 and σ_2). The second step is faster than the fist one ($\sigma_2 > \sigma_1$), and occurs only when a critical dose has been reached. The reduction of AlF_x into metallic aluminum is described by only one cross-section, σ_3, whose value is lower than σ_1 and σ_2.

The energy dependence is correlated with the hole distribution produced by the primary electron. By comparing our experimental results with hole depth distributions calculated by a Monte Carlo simulation, we conclude that the Knotek–Feibelman mechanism, if present, is not certainly the only mechanism responsible of the desorption of fluorine atoms.

Acknowledgements

We are deeply indebted to J. Lugo and E. Goldberg for their help with Gaussian calculations. Professor R. Baragiola is gratefully acknowledged for discussion and valuable suggestions. This work was supported by the ANPCyT (PICT 03-04172) and the U.N.L. (CAI+D 6-6-62).

References

[1] A. Murray, M. Scheinfein, M. Isaacson, I. Adesida, J. Vac. Sci. Technol. B3 (1985) 367.
[2] W. Langheinrich, B. Spangenberg, H. Beneking, J. Vac. Sci. Technol. B10 (1992) 2868.
[3] H. Watanabe, J. Fujita, Y. Ochiai, S. Matsui, M. Ichikawa, Jpn. J. Appl. Phys. 34 (1995) 6950.
[4] S. Chen, C.B. Boothroyd, C.J. Humphreys, Appl. Phys. Lett. 69 (1996) 170.
[5] G.S. Chen, J. Vac. Sci. Technol. A17 (1999) 403.
[6] V.I. Nikolaichik, Philos. Mag. A 68 (1993) 227.
[7] A. Murray, M. Isaacson, I. Adesida, Appl. Phys. Lett. 45 (1984) 589.
[8] G.S. Chen, C.J. Humphreys, J. Vac. Sci. Technol. B 15 (1997) 1954.
[9] M.L. Knotek, P.J. Feibelman, Surf. Sci. 90 (1979) 78.
[10] M. Szymonski, J. Kolodziej, P. Czuba, P. Piatkowski, A. Poradzisz, Phys. Rev. Lett. 67 (1991) 1906.
[11] J. Kolodziej, P. Piatkowski, M. Szymonski, Surf. Sci. 390 (1997) 152.
[12] A. Alexandrov, M. Piacentini, R.G. Tonkyn, M.T. Sieger, N. Zema, T.M. Orlando, Surf. Sci. 451 (2000) 208.
[13] M. Szymonski, J. Kolodziej, Z. Postawa, P. Czuba, P. Piatkowski, Prog. Surf. Sci. 48 (1995) 83.
[14] F. Golek, W.J. Sobolewski, Vacuum 63 (2001) 3.
[15] E. Malinowski, D. Howery, Factor Analysis in Chemistry, Wiley, New York, 1980.
[16] V. Atzrodt, H. Lange, Phys. Status Solidi A 79 (1983) 489.
[17] V. Atzrodt, H. Lange, Phys. Status Solidi A 79 (1984) 373.
[18] R. Vidal, J. Ferrón, Appl. Surf. Sci. 31 (1988) 263.
[19] L. Steren, R. Vidal, J. Ferrón, Appl. Surf. Sci. 29 (1987) 418.
[20] J. Steffen, S. Hofmann, Surf. Sci. 202 (1988) L607.
[21] L.I. Vergara, R.A. Vidal, J. Ferrón, E.A. Sánchez, O. Grizzi, Surf. Sci. 482–485 (2001) 854.
[22] I. Vaquila, M.C.G. Passeggi Jr., J. Ferrón, Phys. Rev. B 55 (1997) 13925.
[23] I. Vaquila, M.C.G. Passeggi Jr., J. Ferrón, Surf. Sci. 292 (1993) L795.
[24] L.I. Vergara, I. Vaquila, J. Ferrón, Appl. Surf. Sci. 151 (1999) 129.
[25] L.I. Vergara, M.C.G. Passeggi Jr., J. Ferrón, Appl. Surf. Sci. 187 (2002) 199.
[26] G. Bushey, C. Eastman, A. Klingsberg, C. Spiro (Eds.), Encyclopedia of Chemical Technology, vol. 10, John Wiley & Sons, 1980, p. 660.
[27] A.F. Trotman-Dickenson et al. (Eds.), Comprehensive Inorganic Chemistry, vol. I, Pergamon Press, 1973, p. 1011.

[28] T.C. Ehlert, J.L. Margrave, J. Am. Chem. Soc. 86 (1964) 3901.
[29] J. Lugo, E. Goldberg, Private Communication, 2002.
[30] R. Vidal, R.A. Baragiola, J. Ferrón, J. Appl. Phys. 80 (1996) 5653.
[31] N.F. Mott, H.S.W. Massey, Theory of Atomic Collisions, third ed., Oxford University, Oxford, 1965, p. 19.
[32] C.J. Powell, A. Jablonski, NIST Electron Inelastic-Mean-Free-Path-Database-Version 1.1, National Institute of Standards and Technology, Gaithersburg, MD (2000).